Density-functional theory modeling of bulk magnetism with spin-dependent pseudopotentials

Frank Starrost,[1] Hanchul Kim,[2] Stuart C. Watson,[1] Efthimios Kaxiras,[2,3] and Emily A. Carter[1,*]
[1]*Department of Chemistry and Biochemistry, Box 951569, University of California, Los Angeles, California 90095-1569*
[2]*Division of Engineering and Applied Sciences, Harvard University, Cambridge, Massachusetts 02138*
[3]*Department of Physics, Harvard University, Cambridge, Massachusetts 02138*
(Received 12 April 2001; published 14 November 2001)

The recently developed spin-dependent pseudopotentials markedly improve the description of the energetics of isolated transition metal atoms [S. C. Watson and E. A. Carter, Phys. Rev. B **58**, R13 309 (1998)]. Spin-dependent pseudopotentials are obtained from a combination of spin-neutral and fully polarized atomic pseudopotentials, employing the self-consistent local spin polarization to adapt to different environments. Their use is extended to bulk materials in the current work, where we have implemented the spin-dependent pseudopotential formalism within a real-space density functional theory code. Calculations on bulk Fe, Co, and Ni yield lattice constants and bulk moduli within the accuracy expected of a method employing the local density approximation of density functional theory, except for an overestimated Fe bulk modulus. However, the magnetic moment is in dramatically better agreement with experiment and published all-electron calculations when the spin-dependent pseudopotentials are employed.

DOI: 10.1103/PhysRevB.64.235105 PACS number(s): 71.15.Dx, 71.15.Mb, 71.15.Nc

I. INTRODUCTION

A large and diverse class of methods for the calculation of the electronic structure of materials depends on pseudopotentials for the description of the interaction of the valence electrons with the nucleus and the core electrons. The use of pseudopotentials simplifies electronic structure calculations considerably, reducing the complexity of the codes and the size of the required computational resources. At the same time, solid state calculations, usually performed within the local density approximation (LDA) (Ref. 1) of density functional theory (DFT),[2] have been shown to accurately predict a number of physical properties for a large variety of materials.

The aim of pseudopotentials is to eliminate the Coulomb singularity of the nuclear potential and the atomic core states while retaining as much of the physical properties outside of the core region as possible. Ever since the introduction of pseudopotentials,[3,4] the determination of the optimum potential for a given atom has been problematic. In addition to describing the atom correctly, the potential should also be ''transferable'' to other chemical environments. Early approaches to the derivation of pseudopotentials from ''first principles'' were based on the orthogonalized plane wave method.[5,6] The introduction of the concept of norm conservation by Topp and Hopfield,[7] Redondo, Goddard, and McGill,[8] and by Hamann, Schlüter, and Chiang[9] has allowed the derivation of smooth pseudopotentials with a very small number of parameters and has led to widespread use of these so-called *ab initio* pseudopotentials. The introduction of the nonlocal form for the pseudopotentials[10] and later refinements of the formalism for the generation of smooth norm-conserving potentials[11] have made the application of pseudopotentials in plane-wave electronic structure codes increasingly straightforward and popular. Ultrasoft pseudopotentials[12] add some complexity to the formalism but can further reduce the computational burden since they require basis sets that are considerably smaller.

The so-called *ab initio* approach can be criticized on several levels, however. For one, the use of DFT requires an approximation to the exchange-correlation functional that is arbitrary to some extent (a problem that affects all-electron as well as pseudopotential DFT methods). The dependence of the exchange-correlation energy on the electron density can be approximated for the uniform interacting electron gas from quantum Monte Carlo calculations, for example.[13,14] However, the fact that there still is an active industry involved in constructing functionals for the LDA (Ref. 15) or the generalized gradient approximation (GGA) (Ref. 16) shows that such a mapping is not unique (despite the unique constraints placed by the uniform gas results) and that a systematic means for their improvement is lacking. Current research in density functional approximations tries to go beyond the limited LDA and GGA forms (see, e.g., Kurth *et al.*[17]).

Also, the pseudopotential formalism has some practical and fundamental problems. On the practical side, the description of atoms with strongly localized valence states, such as oxygen or first-row transition elements, is difficult using norm-conserving pseudopotentials. The description of both their potentials, which are very deep, and the valence states is very costly in plane-wave methods. Ultrasoft pseudopotentials relax the rules of pseudopotential construction to some extent and deliver smooth pseudopotentials that are easily described by plane waves. On the fundamental side, these pseudopotentials are based on a number of parameters that are arbitrary to some extent and call the designation *ab initio* into question.

For the norm-conserving, nonlocal pseudopotential of a first-row transition element, typically four parameters have to be adjusted (ignoring for the moment the ''nonlinear core correction''). These are the three radii for the *s*, *p*, and *d* potentials beyond which the atomic wave functions are to coincide with the all-electron solution, and the choice of the so-called local potential. The local potential is introduced in semilocal and nonlocal pseudopotential approaches. All com-

ponents in the angular momentum decomposition of the wave function experience the local potential. The main components of the wave function, such as those of *s*, *p*, and *d* character, are projected out and for them the potential is corrected to give each their respective potential. All the components of the wave function with $l>2$ experience only the local potential. Typical choices for the local part are one of the *s*, *p*, and *d* potentials, a mix of these, or the all-electron potential whose potential in the inner region is replaced by a Bessel-like function (involving another radius parameter that can be adjusted, see, e.g., Ref. 18).

Pseudopotentials constructed according to the constraint of norm conservation (i.e., the solution for a given *l* at the eigenenergy must have the same charge for both the pseudopotential and the all-electron cases) have relatively deep potentials near the nuclear position for strongly localized states, such as the *d* state in first-row transition metals. As mentioned above, this leads to expensive calculations. One way to avoid this problem is to choose a cutoff radius beyond the outermost maximum of the atomic wave function. Surprisingly, this often leads to physically reasonable results in calculations of ground state bulk properties.

Another way to reduce the computational burden is the ultrasoft pseudopotential (USPP) approach in which the norm-conservation constraint is relaxed so as to produce a smoother potential. Any charge differences are compensated using an augmentation charge density. The new scheme introduces additional parameters: In the original formulation by Vanderbilt[12] these are additional energies, for which the scattering properties of the pseudopotential agree with those of the all-electron potential. These additional energy parameters can be chosen for each angular momentum quantum number *l* independently. The ultrasoft pseudopotentials as employed by Moroni *et al.*[18] have an additional augmentation radius for each *l*, which generally is chosen to be smaller than the cutoff radius. These authors also stress that ''considerable care has to be taken in the construction of the local'' pseudopotential. Their choice is to replace the all-electron potential by a function $A\sin(q_{\mathrm{loc}}r)$ (A and q_{loc} are determined to give a smooth continuation of the all-electron potential) inside a cutoff radius, which is another parameter. In summary, a nonlocal ultrasoft pseudopotential for *s*, *p*, and *d* states, derived from two energies requires three cutoff radii at each energy (six parameters, but usually only one parameter per *l* channel is used) and three augmentation radii (another three parameters), plus the cutoff radius for the local potential (one more parameter). So far, up to ten parameters are required for the definition of the potential.

While norm-conserving and ultrasoft pseudopotentials have been used for a wide range of materials, they fail dramatically in certain cases. One class of examples are open-shell atoms, such as transition metals. Porezag and coworkers report, with reasonable choices of parameters, an error of about 7 eV in the Mn atom spin-polarization energy,[19] the energy difference between the spin-averaged reference state used in the construction of the pseudopotential and the (generally spin-polarized) atomic ground state. The bulk properties of Fe calculated with a norm-conserving pseudopotential by Cho and Scheffler[20] yielded reasonable values for structural parameters such as a bulk lattice constant of 5.54 a.u. (experimental value: 5.42 a.u.) and a bulk modulus of 1.24 Mbar (1.68 Mbar). However, the magnetic moment per atom was significantly too high at $3.09\mu_B$ compared to the experimental value $2.2\mu_B$.

There are a number of reasons for the failure of conventional pseudopotentials. Among them is that they are usually constructed from spin-neutral (equal number of up and down spins) reference configurations. For nearly closed shell atoms, this should be a reasonable approximation, but for highly spin-polarized atoms with large numbers of unpaired electrons or for atoms whose spin configuration changes with environment, such a pseudopotential will provide a poor description of the valence electrons.

Another source of error is the implicit linearization of the exchange-correlation potential in the case of pseudopotentials. The fix frequently employed to overcome the problem is the nonlinear core correction (NLCC).[21] This correction comes with another adjustable parameter, the radius up to which the core density will be replaced by a smoother density for use in plane-wave methods. Using the full core in the NLCC eliminates the linearization error, but the sharp core density cannot be handled efficiently by plane-wave methods. The initial suggestion for the choice of the NLCC radius was the radius where the core and valence density are equal.[21] This fails for many transition metals, as has been demonstrated.[19,22] Porezag *et al.* have pointed out that reducing the core radius (ideally to 0) indeed improves the results for transition metals.[19] However, the sharper core density requires a higher resolution which leads to a higher computational price, particularly in bulk calculations. An alternative approach that allows the treatment of the full core charge is the use of a linear augmented plane wave (LAPW) basis set in combination with pseudopotentials.[20] (The LAPW method is capable of treating the full Coulombic nuclear potential, however.[23])

Another problem of the NLCC is that the LDA exchange potential includes an error when the core density is taken into account because the exchange between valence electrons in the core region is unphysically reduced by a factor of $\frac{1}{3}(\rho^v/\rho^c)^{2/3}$ [where ρ^v (ρ^c) is the valence (core) charge density] from the exchange interaction they would have seen in the absence of core electrons.[24]

In summary, the USPP technique—achieving smoother potentials—in connection with the NLCC—correcting the nonlinear density dependence of the exchange-correlation potential—can give excellent results at a low computational cost. However, there is considerable reason to call into doubt the label ''first principles'' or ''*ab initio*'' for this approach.

In this paper, we demonstrate that the spin-dependent pseudopotentials, which have been shown to dramatically improve the description of the electronic properties of transition metal atoms, give an improved description of transition metal crystal properties as well. In contrast to the USPP, no additional parameters are introduced, the method is thus considerably closer to the *ab initio* spirit. Their drawback is certainly the higher cost compared to USPP, since they retain the property of norm conservation. The results have been obtained from a modified version of the adaptive-coordinate

real-space DFT code (ACRES),[25] high-performance-FORTRAN adaptive grid real-space electronic structure (HARES).[26] In Sec. II, we briefly review the theory of spin dependence for pseudopotentials and the nonlinear core correction, and we introduce HARES. In Sec. III A, results obtained with an atomic code are compared with atomic results obtained using HARES to verify our implementation. Section III B presents results for the bulk properties of transition-metal crystals Fe, Co, and Ni. All calculations are carried out in the local spin density approximation of density functional theory.

II. THEORY

Within the local spin density approximation (LSDA) (Ref. 27) of DFT,[2] the effective potential $v_{\rm eff}^{\sigma}$ for electrons of spin σ in the single-electron Hamiltonian is given by

$$v_{\rm eff}^{\sigma}(\vec{r}) = v_{\rm ext}(\vec{r}) + v_{e\text{-}e}[\rho(\vec{r})] + v_{\rm xc}^{\sigma}[\rho^{\uparrow}(\vec{r}),\rho^{\downarrow}(\vec{r})], \quad (1)$$

where $v_{\rm ext}$ is the external potential, generally the potential due to the nuclei, $v_{e\text{-}e}$ is the classical Coulomb repulsion potential between the electrons, $v_{\rm xc}$ is the electron exchange-correlation potential, $\rho^{\uparrow}$ ($\rho^{\downarrow}$) is the density of the electrons with up (down) spin, and ρ is the total charge density. In the pseudopotential approach, the external potential and the potential due to the core electrons are represented by a smooth, nonsingular potential $v_{\rm ion}$, often called the bare-ion potential because it represents the potential of the atom stripped of its valence electrons. The pseudopotential is constructed to be amenable to a plane-wave representation and is designed to yield solutions to the Kohn-Sham equations[1] that correctly represent the scattering properties (given by the logarithmic derivative of the wave functions) of the valence electrons. The first pseudopotential implementation of the LSDA by Zunger[28] used two distinct ionic pseudopotentials for the up and down spin electrons. However, the most commonly used form[21] employs a single bare-ion pseudopotential $v_{{\rm ion},l}$ for each angular momentum quantum number l. The effective norm-conserving[9] pseudopotential $v_{{\rm eff},l}^{{\rm ps},\sigma}$ for angular momentum l and spin σ is achieved by adding the screening potential due to the valence electrons and then depends on the spin only through $v_{\rm xc}$

$$v_{{\rm eff},l}^{{\rm ps},\sigma}(\vec{r}) = v_{{\rm ion},l}(\vec{r}) + v_{e\text{-}e}[\rho^{v}(\vec{r})] + v_{\rm xc}^{\sigma}[\rho^{v,\uparrow}(\vec{r}),\rho^{v,\downarrow}(\vec{r})], \quad (2)$$

where ρ^{v} ($\rho^{v,\sigma}$) represents the total (σ spin) valence charge density.

For transition metals, this approach typically is used in connection with the NLCC.[21] The NLCC is designed to overcome the implicit linearization of $v_{\rm xc}$ in terms of the core and valence charge densities, in regions where both densities have appreciable value. We will discuss the NLCC in more detail after introducing the necessary variables.

Recently, spin-dependent pseudopotentials have been developed[22] where the bare-ion potential $v_{{\rm ion},l}^{\sigma}$ depends on the spin σ but is not constant for a given atom, as in Zunger's case.[28] Rather, the new $v_{{\rm ion},l}^{\sigma}$ depends on the environment through the spin polarization

$$\beta(\vec{r}) = \frac{\rho^{v,\uparrow}(\vec{r}) - \rho^{v,\downarrow}(\vec{r})}{\rho^{v}(\vec{r})}. \quad (3)$$

It has been shown that the use of these pseudopotentials considerably improves the total energy differences between different spin states of first and second row transition metal atoms, as well as the eigenvalue spectrum across spin states, when compared to all-electron results.[22]

A. Construction of spin-dependent pseudopotentials

No new parameters beyond those of the conventional spin-neutral pseudopotential are introduced in the construction of these spin-dependent pseudopotentials. The process starts with the construction of two screened pseudopotentials. One way to construct these is by first creating the (nodeless) radial part of an atomic pseudowave function $\tilde{\phi}_l^{\sigma}$ from the all-electron wave function according to the norm-conservation criteria.[9,11] Then, with the all-electron orbital energies ϵ_l^{σ}, one can invert the radial Schrödinger equation to obtain the screened pseudopotential $v_{{\rm scr},l}^{\sigma}$, the effective atomic potential of Eq. (2), for the atom at the origin and $r = |\vec{r}|$,

$$v_{{\rm scr},l}^{\sigma}(r) = \epsilon_l^{\sigma} - \frac{l(l+1)}{r^2} + \frac{1}{r\tilde{\phi}_l^{\sigma}(r)}\frac{d^2}{dr^2}[r\tilde{\phi}_l^{\sigma}(r)]. \quad (4)$$

The "bare ion" (due to the nucleus and the core electrons) potential is obtained by unscreening $v_{{\rm scr},l}^{\sigma}$ by subtracting the valence electron repulsion terms

$$v_{{\rm ion},l}^{\sigma}(r) = v_{{\rm scr},l}^{\sigma}(r) - v_{e\text{-}e}[\rho_{\rm at}^{v}(r)] - v_{\rm xc}^{\sigma}[\rho_{\rm at}^{v,\uparrow}(r),\rho_{\rm at}^{v,\downarrow}(r)]. \quad (5)$$

For the construction of the spin-dependent pseudopotentials, the ionic potentials of, e.g., Eq. (5) are needed for two spin states of the atom: the usual spin-neutral reference potential $v_{{\rm ion},l}^{0}$ and the majority spin potential of a fully-polarized spin configuration $v_{{\rm ion},l}^{{\rm fp},\uparrow}$. Given the spin polarization of the fully polarized atom $\beta_{\rm at}(r)$ we define[22]

$$\delta v_l(r) = \frac{v_{{\rm ion},l}^{{\rm fp},\uparrow}(r) - v_{{\rm ion},l}^{0}(r)}{\beta_{\rm at}(r)[2-\beta_{\rm at}(r)]}. \quad (6)$$

The bare-ion pseudopotentials for a general charge density distribution and spin polarization $\beta(r)$ are then

$$v_{{\rm ion},l,\beta}^{\uparrow}(r) = v_{{\rm ion},l}^{0}(r) + \beta(r)[2-\beta(r)]\delta v_l(r), \quad (7)$$

$$v_{{\rm ion},l,\beta}^{\downarrow}(r) = v_{{\rm ion},l}^{0}(r) - \beta(r)[2+\beta(r)]\delta v_l(r). \quad (8)$$

If, in a self-consistent calculation, the spin densities change from iteration to iteration, the ionic potentials ($v_{{\rm ion},l,\beta}^{\sigma}$) change with them. Also, the potentials adapt to changing spin distributions due to different spin configurations or environments, implying an improved transferability. The additional term δv_l has been shown to be much smaller than the spin-neutral bare-ion potential $v_{{\rm ion},l}^{0}$ (Ref. 22) and can be viewed as a perturbation to the latter.

It is these pseudopotentials that have been used in the investigation of the atomic properties.[22] However, in band structure calculations, the use of nonlocal, separable pseudopotentials in the Kleinman-Bylander form[10] can significantly reduce the number of integrals that have to be performed for the calculation of the potential contribution to the Hamiltonian matrix. In the nonlocal approach, first a local pseudopotential $v_{\rm local}$ is chosen (see Sec. I). We then define

$$\Delta v_{{\rm ion},l}(r) = v_{{\rm ion},l}(r) - v_{\rm local}(r), \tag{9}$$

where $v_{{\rm ion},l}(r)$ is given, e.g., by Eq. (5). Equivalently, it is $\Delta v^0_{{\rm ion},l}(r) = v^0_{{\rm ion},l}(r) - v^0_{\rm local}(r)$ and $\Delta v^\sigma_{{\rm ion},l}(r) = v^\sigma_{{\rm ion},l}(r) - v^\sigma_{\rm local}(r)$.

For the spin-dependent pseudopotentials, the potential operator is now defined as (we are suppressing the index ion)

$$\hat{v}^\sigma = v^\sigma_{{\rm local},\beta} + \sum_{lm} \frac{|\Delta v^\sigma_{l,\beta}\phi^{\rm ps}_{lm}\rangle\langle\phi^{\rm ps}_{lm}\Delta v^\sigma_{l,\beta}|}{\langle\phi^{\rm ps}_{lm}|\Delta v^\sigma_{l,\beta}|\phi^{\rm ps}_{lm}\rangle}, \tag{10}$$

with $|\phi^{\rm ps}_{lm}\rangle$ an atomic pseudowave function for the spin-neutral potential (an arbitrary, but reasonable choice, given that δv_l is but a small perturbation on v^0_l). For the majority spin ($\uparrow$) and the atom at the origin, we have

$$v^\uparrow_{{\rm local},\beta}(\vec{r}) = v^0_{\rm local}(r) + \beta(\vec{r})[2-\beta(\vec{r})]\delta v_{\rm local}(r), \tag{11}$$

$$\delta v_{\rm local}(r) = \frac{v^{{\rm fp},\uparrow}_{\rm local}(r) - v^0_{\rm local}(r)}{\beta_{\rm at}(r)[2-\beta_{\rm at}(r)]}, \tag{12}$$

$$\Delta v^\uparrow_{l,\beta}(\vec{r}) = \Delta v^0_l(r) + \beta(\vec{r})[2-\beta(\vec{r})]\delta\Delta v_l(r), \tag{13}$$

$$\delta\Delta v_l(r) = \frac{\Delta v^{{\rm fp},\uparrow}_l(r) - \Delta v^0_l(r)}{\beta_{\rm at}(r)[2-\beta_{at}(r)]}, \tag{14}$$

where each Δv term has the appropriate local potential removed. [The minority spin equivalents of Eqs. (11) and (13) are determined with the signs as in Eq. (8).]

For an atomic calculation, this approach is very similar to the separate treatment for each angular momentum quantum number l [up to an $l_{\rm max}$ which is the upper limit of the sum over l in Eq. (10)]. In the atomic case, for each spin state, the operation of $\hat{v}$ onto an atomic pseudowave function $|\phi^{\rm ps}_{lm}\rangle$ yields

$$\hat{v}|\phi^{\rm ps}_{lm}\rangle = (v_{{\rm local},\beta} + \Delta v_{l,\beta})|\phi^{\rm ps}_{lm}\rangle = v_{l,\beta}|\phi^{\rm ps}_{lm}\rangle. \tag{15}$$

In Eq. (15), the spherical harmonic angular dependence of the atomic pseudowave function $|\phi^{\rm ps}_{lm}\rangle$ projects out the respective symmetry contribution from the Kleinman-Bylander projector $|\Delta v_{l,\beta}\phi^{\rm ps}_{lm}\rangle$. The $\Delta v_{l,\beta}$ are radial functions only, leading to $\langle\phi^{\rm ps}_{lm}\Delta v_{l,\beta}|\vec{r}\rangle = \phi^{\rm ps}_{lm}(r)\Delta v_{l,\beta}(r)Y_{lm}(\hat{\vec{r}})$, where $\hat{\vec{r}} = \vec{r}/r$. It should be noted, however, that Eq. (15) does not hold exactly for an operation on any function of lm symmetry, $\phi'(r)Y_{lm}(\hat{\vec{r}})$. The cancellation of the normalization factor in the denominator of the nonlocal projectors in Eq. (10) depends on the radial part of the function being that of the eigenfunction $|\phi^{\rm ps}_{lm}\rangle$.

In general, however, the projectors in the potential operator $\hat{v}$ constructed according to Eq. (10) contain $\Delta v_{l,\beta}$ that have an angular dependence of their own through Eq. (13) because β is not a radial function as in the special case of the atom. In this case, the projectors will no longer have just a single spherical harmonic angular dependence. The real-space representation of a projector function is

$$\langle\phi^{\rm ps}_{lm}\Delta v_{l,\beta}|\vec{r}\rangle = \phi^{\rm ps}_{lm}(r)\Delta v_{l,\beta}(\vec{r})Y_{lm}(\hat{\vec{r}}) \tag{16}$$

$$= \phi^{\rm ps}_{lm}(r)\Delta v^0_l(r)Y_{lm}(\hat{\vec{r}}) + \beta(\vec{r}) \times[2-\beta(\vec{r})]\phi^{\rm ps}_{lm}(r)\delta\Delta v_l(r)Y_{lm}(\hat{\vec{r}}). \tag{17}$$

The spherical harmonic Y_{lm}, which is used to project out the lm component from a wave function applied to $\hat{v}$, may be distorted in the second term of Eq. (17) when β deviates from spherical symmetry. The orthonormality of the spherical harmonics will then no longer ensure strictly that each lm component will only "see" its appropriate pseudopotential $v_{l,\beta}$. Yet, since $|\delta\Delta v_l(r)| \ll |\Delta v^0_l(r)|$ in the radial interval where they are not negligible (see Fig. 3 of Ref. 22), we have

$$\hat{v}|\phi^{\rm ps}_{lm}\rangle \approx (v_{{\rm local},\beta} + \Delta v_{l,\beta})|\phi^{\rm ps}_{lm}\rangle = v_{l,\beta}|\phi^{\rm ps}_{lm}\rangle. \tag{18}$$

One aim of this study is to investigate whether this approximation diminishes the quality of the results.

B. Nonlinear core correction

The exchange-correlation potential $v_{\rm xc}$ is a nonlinear function of the density. Since only the valence electrons are treated in pseudopotential calculations, only the valence density is readily available for the calculation of $v_{\rm xc}$. The $v_{\rm xc}$ due to the core electrons is "included" in the pseudopotential. This separation means that the potential has been effectively linearized with respect to core and valence density, an approximation that is problematic in regions of space where both densities are of appreciable value. To remedy this problem Louie *et al.* introduced the "nonlinear core correction,"[21] which is described here.

In the conventional treatment, the bare ion potential $v^\sigma_{{\rm ion},l}$ is constructed from the atomic potential, using the atomic valence density $\rho^v_{\rm at}$. For the sake of clarity, we will ignore the spin dependence in this subsection. Then the bare potential is, according to Eq. (5),

$$v_{{\rm ion},l}(r) = v_{{\rm scr},l}(r) - v_{e\text{-}e}[\rho^v_{\rm at}(r)] - v_{\rm xc}[\rho^v_{\rm at}(r)]. \tag{19}$$

The screened potential $\tilde{v}_{{\rm scr},l}$ in a different environment (a different spin state of the atom, in a molecule or solid) with valence density ρ^v is (for the atom at the origin, with $r = |\vec{r}|$)

$$\tilde{v}_{{\rm scr},l}(\vec{r}) = v_{{\rm ion},l}(r) + v_{e\text{-}e}[\rho^v(\vec{r})] + v_{\rm xc}[\rho^v(\vec{r})]. \tag{20}$$

Then, according to this procedure, the total exchange-correlation potential $\tilde{v}_{\rm xc}$ in the different environment is implicitly

$$\tilde{v}_{\rm xc}(\vec{r})=\{v_{\rm xc}[\rho^v_{\rm at}(r)+\rho^c_{\rm at}(r)]-v_{\rm xc}[\rho^v_{\rm at}(r)]\}+v_{\rm xc}[\rho^v(\vec{r})]. \quad (21)$$

However, due to the nonlinearity of the exchange-correlation potential, it is the case that

$$\{v_{\rm xc}[\rho^v_{\rm at}(r)+\rho^c_{\rm at}(r)]-v_{\rm xc}[\rho^v_{\rm at}(r)]\}\neq v_{\rm xc}[\rho^c_{\rm at}(r)]. \quad (22)$$

It means that the term in curly brackets depends on the valence configuration used to determine $v_{{\rm scr},l}$ according to Eq. (4). This dependence reduces the transferability of the potential. Additionally, this procedure leads to (for simplicity, we assume here that the core is frozen, i.e., it does not change in a different chemical environment)

$$\tilde{v}_{\rm xc}(\vec{r})\neq v_{\rm xc}[\rho^v(\vec{r})+\rho^c_{\rm at}(r)], \quad (23)$$

for all $\vec{r}$ except those with

$$\rho(\vec{r})=\rho^v_{\rm at}(r) \quad (24)$$

or

$$\rho^v_{\rm at}(r)=0 \ \text{ and } \ \rho^v(r)=0, \quad (25)$$

$$\rho^c_{\rm at}(r)=0. \quad (26)$$

In the first case [Eq. (24)], two potential contributions are trivially subtracted and added to cancel exactly, in the latter two cases [Eqs. (25) and (26)] the nonlinearity of $v_{\rm xc}$ does not affect the result [see Eq. (21)].

For a charge distribution in an atom described by pseudopotentials (see Fig. 2 for an example), the condition expressed in Eq. (25) is met approximately near the nucleus [where $\rho^v_{\rm at}(r)\approx\rho^v(r)\ll\rho^c_{\rm at}(r)$] and condition (26) is met far away from the nucleus. However, the error made in the construction of $\tilde{v}_{\rm xc}$ is noticeable in regions of space where both the valence and the core density have appreciable value.

To improve the situation, Louie *et al.* suggested the ''nonlinear core correction.''[21] The idea is that in the construction of the bare ion potential, the exchange-correlation potential of the total charge is subtracted from the screened potential, rather than the $v_{\rm xc}$ due to the valence charge only. This then avoids linearization of the $v_{\rm xc}$. Since the core charge is strongly peaked, so is the $v_{\rm xc}[\rho^v_{\rm at}(r)+\rho^c_{\rm at}(r)]$. However, strongly peaked functions are difficult to represent in a plane wave basis or on a real-space grid. For this reason, the ionic potential instead is calculated according to

$$v_{{\rm ion},l}(r)=v_{{\rm scr},l}(r)-v_{e\text{-}e}[\rho^v_{\rm at}(r)]-v_{\rm xc}[\rho^v_{\rm at}(r)+\rho^c_{\rm at,smooth}(r)]. \quad (27)$$

The charge density $\rho^c_{\rm at,smooth}$ agrees with the real core charge density outside a radius $r_{\rm core}$ but has been smoothed in the interval $[0,r_{\rm core}]$. The radius $r_{\rm core}$ should be chosen such that the valence charge density is negligible within this radius. The screened potential is then calculated as

$$\tilde{v}_{{\rm scr},l}(\vec{r})=v_{{\rm ion},l}(r)+v_{e\text{-}e}[\rho^v(\vec{r})]+v_{\rm xc}[\rho^v(\vec{r})+\rho^c_{\rm at,smooth}(r)]. \quad (28)$$

The justifications for using Eq. (28) to calculate the exchange-correlation potential are different outside and inside the core radius $r_{\rm core}$. For $r>r_{\rm core}$, $v_{\rm xc}$ due to the total density $[\rho^v(\vec{r})+\rho^c_{\rm at,smooth}(r)$, which agrees with $\rho^v(\vec{r})+\rho^c_{\rm at}(r)$ in that interval] in the current environment is added after the atomic exchange-correlation potential was removed according to Eq. (27). For $r<r_{\rm core}$, meanwhile, it is assumed that $\rho^v_{\rm at}(r)\approx\rho^v(\vec{r})\approx 0$ and thus the exchange-correlation potential term $v_{\rm xc}[\rho^c_{\rm at,smooth}(r)]$ subtracted in Eq. (27) is added back. Different choices of $r_{\rm core}$ can have a substantial effect on the predicted energies of atoms.[19] Differences in the spin-polarization energies can be as large as 7 eV for Mn depending on the value of $r_{\rm core}$.

C. Implementation

The spin-dependent pseudopotentials as described in Eq. (10) have been implemented into the newer version (HARES) (Ref. 26) of ACRES developed by Modine *et al.*[25] Eigenfunctions, charge densities, and potentials are represented on a real-space grid that can be adapted so as to give a higher density of points near the nuclei. The adaptive grid can be mapped onto a regular grid in curvilinear space, which is important for an efficient parallelization of the code. Adaptability, parallelizability, and the sparsity of the Hamiltonian matrices due to the real-space representation are the prerequisites for efficient electronic structure calculations. HARES has been used to study the basic electronic and structural properties of elemental crystalline solids, molecules, and complex crystalline materials, such as blue bronze and zeolites.[26,29,30]

III. RESULTS AND DISCUSSION

A. The nickel atom

To test the quality of the pseudopotentials used and the correctness of the implementation of the spin-dependent pseudopotentials in HARES, we present results for the Ni atom. We were seeking to reproduce the results of a program based on the code by Troullier and Martins (TM) (Ref. 11) that has been modified to include the spin-dependent pseudopotentials.[22] The TM program takes the spherical symmetry of the atomic problem into account and solves only the radial problem on a one-dimensional grid, whereas HARES solves for the electronic structure on a three-dimensional grid on which full cubic symmetry has been imposed. Additionally, the TM code uses separate potentials for each angular momentum channel and does not use the Kleinman-Bylander projectors [Eq. (10)] employed in HARES. The parameters for the construction of the pseudopotentials used in this investigation are given in Table I. We have calculated the eigenvalues and total energies for the $4s^1 3d^{n-1}$ and $4s^2 3d^{n-2}$ configurations of the Ni atom within the LSDA.

In Table II and Fig. 1 we compare the results of the pseudopotential calculations executed using the atomic TM code and HARES (and we also show the all-electron results). To assess the accuracy that can be expected when comparing

TABLE I. The computational parameters for the atomic calculations are given in the upper panel. For an explanation of the HARES parameters, see Ref. 25. The inverse Jacobians $1/|J|$ are given at the site of the atom and give a combined inverse Jacobian of 64.0. The pseudopotential parameters are given in the lower panel. $r_{c,l}$ are the radii beyond which the pseudowave function is to coincide with the all-electron wave function. PZ refers to Perdew and Zunger, LSDA is the local spin density approximation, and r_{core} is the core radius for the nonlinear core correction.

Box size	$(16$ a.u.$)^3$		
Grid size (HARES)	$80\times80\times80$		
Global backdrop (HARES)	Size: $(5$ a.u.$)^3$, $1/\|J\|=2.0^3$		
Local adaptation (HARES)	$1/\|J\|=8.0$, $\kappa=1.0$ a.u.		
Exchange-correlation potential	PZ (Ref. 14) (LSDA)		
Atom	Fe	Co	Ni
$r_{c,s}$ (a.u.)	2.26	2.18	2.10
$r_{c,p}$ (a.u.)	3.05	2.98	2.91
$r_{c,d}$ (a.u.)	2.00	2.18	2.08
r_{core} (a.u.)			0.60

the results from the two very different codes, the values for the conventional spin-neutral potential are compared first. (At this point we are not primarily concerned with the comparison with the all-electron results, which differ significantly, especially for the *d* states. Rather, the comparison is between the TM and the HARES results.) The occupied orbital eigenenergies agree to within 0.14 eV between the TM and the HARES calculations. The energies of the unoccupied *p* states differ by up to 0.19 eV. Moving to the spin-dependent pseudopotentials now, the maximum differences between the TM atomic code and HARES are <0.16 eV for the occupied and <0.20 eV for the unoccupied states. Note there are systematic differences, such as the *p* states consistently being too high in energy (in HARES) for all cases studied.

The total energy differences (Table II) between the $4s^13d^{n-1}$ and $4s^23d^{n-2}$ configurations in the TM and the HARES calculations are reproduced to within 30 meV in both the spin-neutral and the spin-dependent cases. In the latter case, the result is considerably improved with respect to the all-electron value (within 10 meV).

These observations show that the implementation is correct and that the use of the Kleinman-Bylander operator is justified in the atomic case. Residual errors are due to numerical imprecision. Figure 1 also shows that the use of the spin-dependent pseudopotentials improves the agreement with the all-electron orbital energies considerably compared to the conventional spin-neutral pseudopotentials, as found previously.[22]

These calculations were done without a NLCC, since the primary aim here is to compare results between the atomic code and the three-dimensional real-space program. For some bulk calculations of Ni, the NLCC was used, and the

TABLE II. Comparison of all-electron to pseudopotential DFT calculations of properties [orbital energies, total energies, and state splitting $\Delta E=E_{\text{tot}}(4s^23d^8)-E_{\text{tot}}(4s^13d^9)$]. Energies in eV. AE: all-electron, SN: spin-neutral pseudopotential, SD: spin-dependent pseudopotential calculations, TM: atomic Troullier-Martins code (Ref. 11), HARES: HARES code (Ref. 26). These orbital energies are displayed graphically in Fig. 1.

			$4s^23d^8$				
nl	s	occ.	AE - TM	SN - TM	SN - HARES	SD - TM	SD - HARES
$4s$	↑	1	-5.89	-5.92	-5.90	-5.89	-5.86
$4s$	↓	1	-5.58	-5.56	-5.55	-5.58	-5.55
$4p$	↑	0	-1.43	-1.43	-1.32	-1.43	-1.31
$4p$	↓	0	-1.32	-1.33	-1.20	-1.33	-1.20
$3d$	↑	5	-10.31	-10.80	-10.80	-10.31	-10.24
$3d$	↓	3	-8.47	-7.86	-7.85	-8.45	-8.39
E_{tot}			-40952.28	-948.71	-948.82	-948.15	-948.26
			$4s^13d^9$				
nl	s	occ.	AE - TM	SN - TM	SN - HARES	SD - TM	SD - HARES
$4s$	↑	1	-4.91	-4.92	-4.98	-4.92	-4.96
$4s$	↓	0	-4.03	-4.03	-4.09	-4.01	-4.07
$4p$	↑	0	-1.05	-1.06	-0.952	-1.06	-0.952
$4p$	↓	0	-0.517	-0.544	-0.354	-0.530	-0.326
$3d$	↑	5	-5.45	-5.48	-5.62	-5.22	-5.29
$3d$	↓	4	-4.46	-4.00	-4.12	-4.28	-4.37
E_{tot}			-40953.84	-949.74	-949.82	-949.62	-949.72
ΔE			1.56	1.03	1.00	1.47	1.46

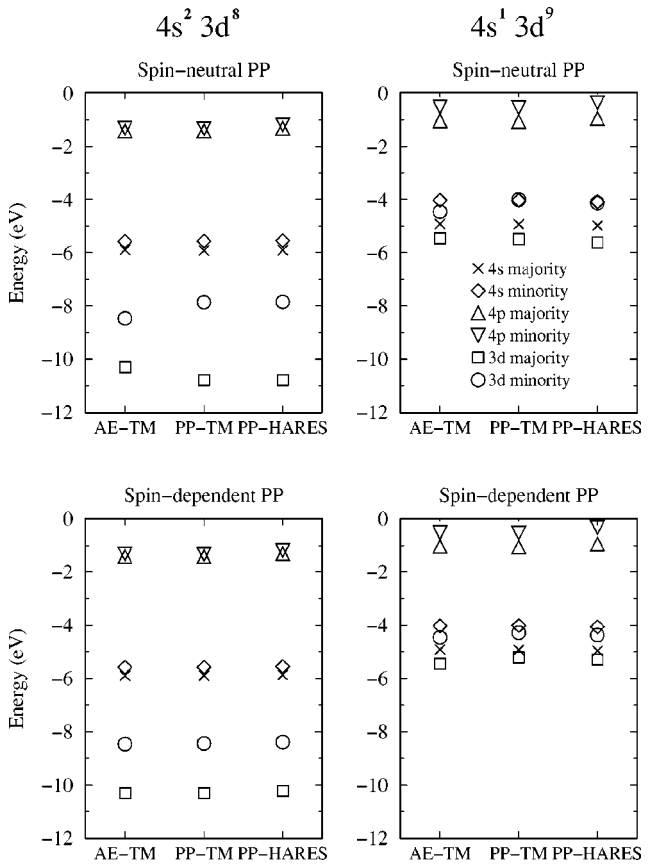

FIG. 1. Orbital energies for the $4s^2 3d^8$ and $4s^1 3d^9$ configurations of the Ni atom calculated with an all-electron atomic code (AE-TM), a pseudopotential atomic code (PP-TM) and an adaptive coordinate real space program (PP-HARES). Calculations are presented for spin-neutral and spin-dependent pseudopotentials. The aim here is to show that the implementation of the spin-dependent real-space Kleinman-Bylander approach (PP-HARES) reproduces the atomic results (PP-TM) with the same accuracy as for the spin-neutral pseudopotential. The results also show the improvement in the orbital energies—compared to the all-electron results—when the spin-dependent pseudopotential is switched on for both configurations. In the panel for the $4s^1 3d^9$ configuration calculated with spin-neutral pseudopotentials, the $4s$ and $3d$ minority symbols lie on top of each other. For the numeric values, see Table II.

choice of the radius r_{core} within which the real core charge density is replaced by the smoother partial density is illustrated in Fig. 2. The aim is to choose r_{core} as small as possible so as to describe the core charge density correctly in the region where the valence charge density is not negligible. At the same time, r_{core} may not be too small because then the representation of the strongly peaked core charge will be difficult for, e.g., plane-wave or real-space grid methods such as HARES. For that reason, in the case shown in Fig. 2, the choice was $r_{\mathrm{core}}=0.6$ a.u. A simple formula that calculates the core radius as half the sum of the cutoff radius and the radius to the first node[19] would give r_{core} of 1.04 a.u. in the case of Ni. Figure 2 shows that such a radius ($r_{\mathrm{core}}=1.1$ a.u.) is much too large for the current case: The core charge is misrepresented very strongly in the region where core charge density and valence charge density are of comparable size. The reason lies in the large cutoff radius for the d orbital, which is necessary to achieve a smooth norm-conserving pseudopotential.

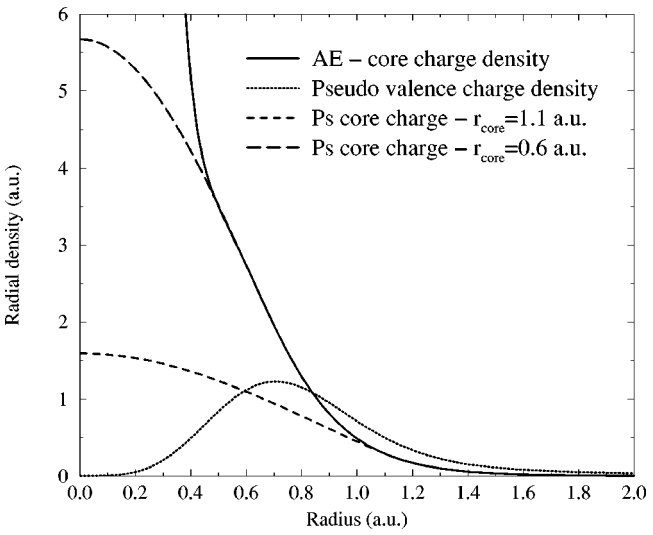

FIG. 2. The charge density distribution in the Ni atom. The all-electron (AE) core charge density is shown by a solid line; the pseudo valence density is depicted by a dotted line. Pseudo (Ps) core charge distributions for the nonlinear core correction are shown for two cutoff radii r_{core}: 1.1 and 0.6 a.u.

B. Crystal results

The spin-dependent pseudopotentials[22] are expected to be most important for the magnetic transition metals Fe, Co, and Ni. To evaluate the effect of the spin-dependent pseudopotentials on the properties of these magnetic materials, we have calculated the bulk lattice constant a, bulk modulus B, and magnetic moment M (also called the saturation magnetization) within the LSDA, using the exchange-correlation functional as parametrized by Perdew and Zunger.[14] The computational parameters are given in Table III. (Convergence tests showed that the resolution of the grid and the number of $\vec{k}$ points were sufficient.) The results were calculated with the spin-neutral and the spin-dependent pseudopotentials described in Table I without using a NLCC. The computational effort for the spin-dependent pseudopotential

TABLE III. The computational parameters for bulk calculations. For an explanation of the HARES adaptation parameters, see Ref. 25. The lattice constant a refers to the conventional cubic cell, IBZ stands for the irreducible part of the Brillouin zone, PZ is Perdew and Zunger.

Unit cell	Conventional cubic cell
Atoms per unit cell	fcc: 4, bcc: 2
Box size	a^3
Grid size	40×40×40
No. $\vec{k}$ points in IBZ	20
Local adaptation	$1/\lvert J\rvert=8.0$, $\kappa=0.9$ a.u.
Exchange-correlation potential	PZ (Ref. 14) (LSDA)

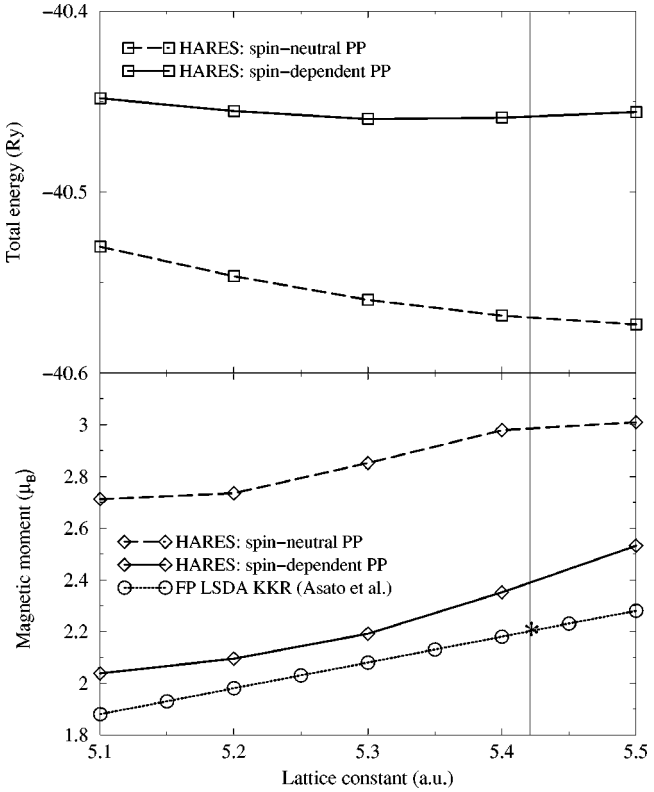

FIG. 3. The upper panel shows the total energy per atom (Ry) at different lattice constants for spin-neutral and spin-dependent pseudopotentials for Fe. In the lower panel, the magnetic moment per atom is displayed for the spin-neutral and the spin-dependent pseudopotentials. For comparison, all-electron full-potential KKR DFT-LSDA results are also shown (Ref. 31). All results were calculated using the LSDA with the exchange-correlation potential parametrized by Perdew and Zunger (Ref. 14). The experimental lattice constant is indicated by the vertical line and the experimental magnetic moment per atom (Ref. 36) by an asterisk.

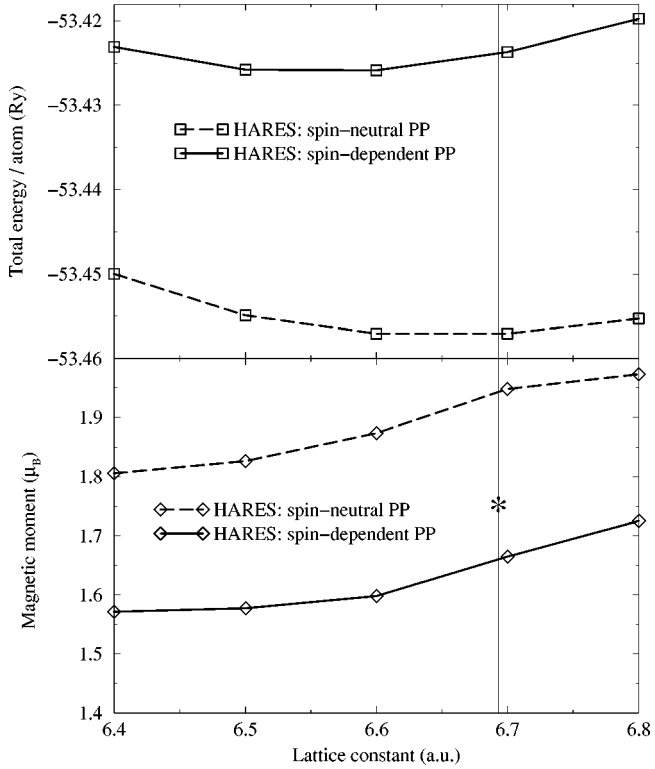

FIG. 4. The upper panel shows the total energy per atom (Ry) at different lattice constants for Co calculated with spin-neutral and spin-dependent pseudopotentials. In the lower panel, the magnetic moment per atom is displayed for the spin-neutral and the spin-dependent pseudopotentials. All results were calculated using the LSDA with the exchange-correlation potential parametrized by Perdew and Zunger (Ref. 14). The experimental lattice constant is indicated by the vertical line and the experimental magnetic moment per atom (Ref. 36) by an asterisk.

calculations did not increase noticeably compared with the equivalent spin-neutral ones.

The dependence of the total energy and the magnetic moment on the lattice constant for bcc Fe, fcc Co, and fcc Ni is displayed in Figs. 3, 4, and 5, respectively. For comparison purposes, we also show all-electron full-potential Korringa-Kohn-Rostoker (KKR) DFT-LSDA results,[31] which were available for Fe and Ni. The properties derived from these curves (bulk lattice constant, the bulk modulus and the magnetic moment at the LSDA equilibrium lattice constant) are given in Tables IV, V, and VI and compared to the experimental and other theoretical values. The experimental magnetic moment per atom is the figure extrapolated to 0 K. The lattice constant and bulk modulus have been measured at room temperature, but the values at 0 K should differ only slightly since their coefficients of thermal expansion are small.

The pseudopotential parameters were chosen so as to yield correct lattice constants a and reasonable bulk moduli B for the spin-dependent pseudopotential result. In particular, the cutoff radius for the d potential was chosen so as to give a lattice constant that is slightly too small for the spin-dependent pseudopotentials, as would be expected for an LDA calculation (needless to say, this is not a very satisfactory approach for an ''*ab initio*'' method). Our reasoning here is to set up a pseudopotential that will yield correct physics with regard to the lattice constant, and then to determine the magnetic moment for this pseudopotential.

For the spin-dependent pseudopotentials, we find equilibrium lattice constants that are within the range given by either all-electron or ultrasoft pseudopotential methods. As shown in Table IV, for Fe, the spin-dependent pseudopotentials yield a lattice constant of 5.35 a.u., which is less than the experimental value of 5.42 a.u. but closer than the all-electron (5.20 a.u.) and the USPP with NLCC result (5.22 a.u.). For Co, the spin-dependent result is 6.56 a.u., which is below the experimental value of 6.70 a.u. but close to the all-electron result of 6.54 a.u. and the USPP with NLCC with 6.52 a.u., see Table V. The Ni lattice constant obtained with spin-dependent pseudopotentials of 6.57 a.u. is below the experimental value of 6.66 a.u., but closer than the all-electron results of 6.46 a.u. and the value obtained by the USPP with NLCC of 6.48 a.u., see Table VI. These results suggest we choose an adequate set of pseudopotential parameters. Comparing the lattice constants obtained with the spin-neutral reference pseudopotential, we find Ni basically un-

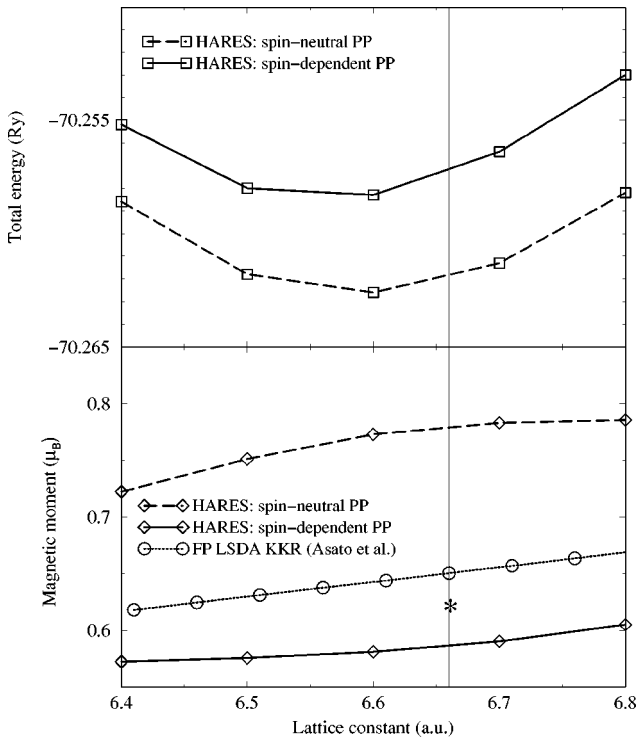

FIG. 5. The upper panel shows the total energy per atom (Ry) at different lattice constants for spin-neutral and spin-dependent pseudopotentials for Ni. In the lower panel, the magnetic moment per atom is displayed for the spin-neutral and the spin-dependent pseudopotentials. For comparison, all-electron full-potential KKR DFT-LSDA results are also shown (Ref. 31). All results were calculated using the LSDA with the exchange-correlation potential parametrized by Perdew and Zunger (Ref. 14). The experimental lattice constant is indicated by the vertical line and the experimental magnetic moment per atom (Ref. 36) by an asterisk.

changed, while Fe and Co differ significantly: Iron is most dramatic—its lattice constant is increased by 4.5% to 5.59 a.u. with the spin-neutral pseudopotential, well above the experimental value of 5.42 a.u.; for fcc Co, the change is from 6.56 to 6.66 a.u., which is still smaller than the experimental result. (A different choice of parameters could have provided the same lattice constant for the spin-neutral pseudopotential—but have changed the magnetic properties negligibly.)

The bulk moduli are virtually identical whether calculated with the spin-dependent or the spin-neutral pseudopotentials (the changes in the modulus are on the order of 2%). For Fe, B is nearly three times the experimental value and about twice what the all-electron and USPP methods yield. We decided not to adjust the pseudopotential further for the purposes of this work. In Co and Ni, we obtain bulk moduli closer to experiment than the other methods throughout.

Comparing the magnetic moment per atom calculated with the spin-dependent pseudopotentials for the three crystals, we note that in Fe our result ($2.28\mu_B$) is markedly closer to the experimental value ($2.2\mu_B$) than the value obtained by all-electron methods ($1.98\mu_B$) or the USPP with NLCC ($2.05\mu_B$). In Co, our result ($1.58\mu_B$) is in between the all-electron value ($1.62\mu_B$) and the USPP with NLCC ($1.52\mu_B$), all of which are smaller than the measured M of $1.75\mu_B$. In Ni, the spin-dependent pseudopotential ($0.57\mu_B$) yields virtually the same result as the USPP with NLCC ($0.59\mu_B$) whereas the all-electron result agrees with the experimental one ($0.62\mu_B$). So, generally, the theoretical magnetic moments tend to be slightly too small compared with experiment and the spin-dependent results do as well as, and sometimes better than, other highly accurate methods.

Considerable changes are seen in the magnetic moment depending on whether the spin-dependent potential is turned on, see Fig. 6. The spin-neutral calculations yield magnetic

TABLE IV. Equilibrium values for the lattice constant a, the bulk modulus B, and the magnetic moment per atom M of bcc Fe calculated by different methods. Also given are the measured values. All calculations were performed within the local spin density approximation to density functional theory using the exchange-correlation potential according to Perdew and Zunger (Ref. 14), except for the all-electron calculations which used different parametrizations. The full-potential Korringa-Kohn-Rostoker (FP KKR) and full-potential linear augmented plane wave (FLAPW) methods are all-electron DFT approaches. The abbreviations are NLCC: nonlinear core correction, SN: spin-neutral, PP: pseudopotential, SD: spin-dependent, LAPW: linear augmented plane wave, FC: full core, USPP: ultrasoft pseudopotentials. The HARES calculations by Waghmare *et al.* (Ref. 26) used a different pseudopotential than the one used here. The magnetic moment is derived by interpolation for the predicted equilibrium lattice constant at each level of theory.

Method	NLCC	a (a.u.)	B (GPa)	M (μ_B)	Source
Experiment	n/a	5.42	167	2.2	(Refs. 34–36)
FP KKR/FLAPW	n/a	5.20 ± 0.02	250 ± 9	1.98	(Ref. 31)
HARES SN PP	no	5.59	432	3.04	This work
HARES SD PP	no	5.35	444	2.28	This work
HARES (Ref. 26)	yes	5.29	201	2.06	(Ref. 26)
LAPW PP	yes (FC)	5.22	226	2.22	(Ref. 20)
USPP	yes	5.22	235	2.05	(Ref. 18)

TABLE V. Equilibrium lattice constant *a*, bulk modulus *B*, and magnetic moment per atom *M* of fcc Co from experiment and calculated by different DFT-LSDA methods. For the abbreviations, see Table IV; LMTO stands for the linear muffin tin orbital (Ref. 23) all-electron DFT technique. All pseudopotential (PP) calculations were done using the exchange-correlation potential according to Perdew and Zunger (Ref. 14).

Method	NLCC	*a* (a.u.)	*B* (GPa)	*M* (μ_B)	Source
Experiment	n/a	6.70	187	1.75	(Refs. 34,36,37)
LMTO	n/a	6.54	255	1.62	(Ref. 38)
HARES SN PP	no	6.66	219	1.92	This work
HARES SD PP	no	6.56	221	1.58	This work
LAPW PP	yes (FC)	6.51	237	1.49	(Ref. 20)
USPP	yes	6.52	242	1.52	(Ref. 18)

moments for all three substances that are overestimated, while the spin-dependent pseudopotentials reduce *M* considerably. In Fe and Co, the spin-dependent results are considerably closer to the experimental value than the spin-neutral values. In Co, the deviation of *M* from experiment is about the same for either spin-dependent or spin-neutral pseudopotentials. Figure 6 also shows that the magnetic moment for Fe and Co are closer to the experiment than those calculated with the USPP, while the results from spin-dependent and ultrasoft pseudopotentials are almost the same for Ni, with the USPP yielding slightly better results.

Comparing the spin-neutral HARES results for Ni with and without NLCC shows that the NLCC yields a slightly larger lattice constant (it goes from 6.59 to 6.66 a.u.) and a significant increase in the bulk modulus (from 209 to 261 GPa) away from the experimental value. A plane-wave DFT-LSDA calculation by Cho and Kang[32] using norm-conserving pseudopotentials finds no change in the lattice constant (6.62 a.u.) and a small increase in the bulk modulus (237 to 243 GPa), by incorporating the NLCC. Both calculations agree about the decrease in the magnetic moment due to NLCC: Cho and Kang find a decrease from 0.78 to $0.66\mu_B$; we see a change from 0.77 to $0.57\mu_B$. The results using the NLCC yield magnetic moments practically identical to the results achieved with the spin-dependent pseudopotentials. Using the spin-dependent rather than the spin-neutral pseudopotentials in combination with the NLCC makes hardly any difference in the bulk results for Ni.

The results show conclusively that in all cases the spin-dependent pseudopotentials reduce the magnetic moment considerably, generally bringing the result closer to the experimental value. This effect was observed to be independent of the quality of the pseudopotential. Even for pseudopotentials created with parameters that did not yield a lattice constant close to the experimental result, the effect of switching on the spin dependence was similar to the one demonstrated here, with the values of *M* and their changes very similar to the results presented. The magnetic moments obtained with the spin-dependent pseudopotentials are of a quality similar, in some cases better, to that of the other pseudopotential methods employing the NLCC.

The use of the spin-dependent pseudopotentials yields similar results regarding the magnetic moment as the application of the NLCC, even though both approaches are very different in nature. The spin-dependent pseudopotentials optimize the ionic pseudopotentials for the valence spin charge densities, whereas the NLCC takes into account the core charge and the nonlinearity of the exchange-correlation potential. In contrast to the spin-dependent pseudopotentials, the NLCC introduces an additional parameter. Additionally, the need for an improved representation for the core density requires considerably higher computational effort for a calculation employing the NLCC.

TABLE VI. Equilibrium lattice constant *a*, bulk modulus *B*, and magnetic moment per atom *M* of fcc Ni from experiment and calculated by different DFT-LSDA methods. For the abbreviations, see Table IV. All pseudopotential (PP) calculations were done with the exchange-correlation potential according to Perdew and Zunger (Ref. 14).

Method	NLCC	*a* (a.u.)	*B* (GPa)	*M* (μ_B)	Source
Experiment	n/a	6.66	184	0.62	(Refs. 34–36)
FP KKR/FLAPW	n/a	6.46	254 ± 2	0.62	(Ref. 31)
HARES SN PP	no	6.59	209	0.77	This work
HARES SD PP	no	6.57	208	0.57	This work
HARES SN PP	yes	6.66	261	0.57	This work
HARES SD PP	yes	6.66	260	0.58	This work
HARES (Ref. 26)	yes	6.58	248	0.57	(Ref. 26)
LAPW PP	yes (FC)	6.50	239	0.60	(Ref. 20)
USPP	yes	6.48	255	0.59	(Ref. 18)
Norm-conserving PP	no	6.62	237	0.78	(Ref. 32)
Norm-conserving PP	yes	6.62	243	0.66	(Ref. 32)

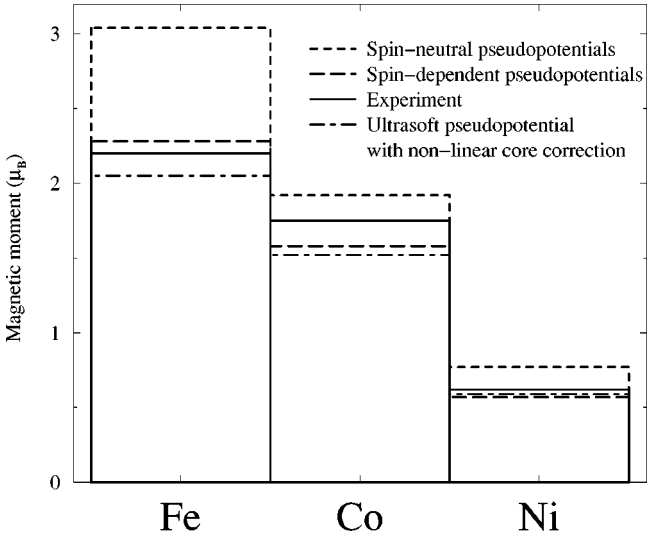

FIG. 6. The magnetic moment per atom calculated using spin-neutral and spin-dependent pseudopotentials for Fe, Co, and Ni. The results are compared to the experimental values (Ref. 36) and magnetic moments from ultrasoft pseudopotential calculations (Ref. 18).

IV. CONCLUSIONS

The spin-dependent pseudopotentials improve the description of magnetic bulk properties of the transition metals Fe, Co, and Ni compared to results from spin-neutral pseudopotentials. The magnetic moment is reproduced with the same quality or better than via the ultrasoft pseudopotential approach in combination with the non-linear core correction without the additional parameters the latter approach requires. These results not only indicate that the spin-dependent pseudopotentials work in a bulk environment but also that the generalized Kleinman-Bylander form, which includes the nonspherical spin polarization [see Eq. (10)], does not adversely affect the description of the physical properties. Using the NLCC for spin-neutral pseudopotentials yields about the same improvement in the magnetic moment as the use of spin-dependent pseudopotentials. The NLCC, however, in contrast to the spin-dependent pseudopotentials, comes at the cost of fitting an additional parameter. Thus, the spin-dependent pseudopotential approach provides an accurate description of bulk properties with a minimum number of adjustable parameters. The cost of this increase in "*ab initio*-ness," however, is the harder nature of the norm-conserving pseudopotentials. These potentials will provide a useful alternative in cases where fitting satisfactory ultrasoft pseudopotentials and core charges for the NLCC becomes tedious, difficult or simply unaesthetic. Introducing spin-dependence would be a way to avoid the arbitrariness of the NLCC for the computationally advantageous ultrasoft pseudopotentials.[33]

ACKNOWLEDGMENTS

Two of us (F.S. and E.A.C.) would like to thank Tim Kaxiras for the hospitality extended to them for several months at Harvard University. This work has been funded in part by the DoD-MURI program, administered by the Air Force Office of Scientific Research, the Army Research Office, and the National Science Foundation. This work was also partially supported by National Computational Science Alliance through computer time on the NCSA SGI/CRAY Origin 2000.

*Email address: eac@chem.ucla.edu; Homepage: http://www.chem.ucla.edu/carter

[1] W. Kohn and L. J. Sham, Phys. Rev. **140**, A1133 (1965).
[2] P. Hohenberg and W. Kohn, Phys. Rev. **136**, B864 (1964).
[3] J. C. Phillips, Phys. Rev. **112**, 685 (1958).
[4] M. L. Cohen and V. Heine, Solid State Phys. **24**, 37 (1980).
[5] C. F. Melius and W. A. Goddard III, Phys. Rev. A **10**, 1528 (1974).
[6] A. Zunger and M. L. Cohen, Phys. Rev. Lett. **41**, 53 (1978).
[7] W. C. Topp and J. J. Hopfield, Phys. Rev. B **7**, 1295 (1973).
[8] A. Redondo, W. A. Goddard III, and T. C. McGill, Phys. Rev. B **15**, 5038 (1977).
[9] D. R. Hamann, M. Schlüter, and C. Chiang, Phys. Rev. Lett. **43**, 1494 (1979).
[10] L. Kleinman and D. M. Bylander, Phys. Rev. Lett. **48**, 1425 (1982).
[11] N. Troullier and J. L. Martins, Phys. Rev. B **43**, 1993 (1991).
[12] D. Vanderbilt, Phys. Rev. B **41**, 7892 (1990).
[13] D. M. Ceperley and B. J. Alder, Phys. Rev. Lett. **45**, 566 (1980).
[14] J. P. Perdew and A. Zunger, Phys. Rev. B **23**, 5048 (1981).
[15] Y. A. Wang, Chem. Phys. Lett. **268**, 76 (1997).
[16] J. P. Perdew, K. Burke, and M. Ernzerhof, Phys. Rev. Lett. **77**, 3865 (1996).
[17] S. Kurth, J. P. Perdew, and P. Blaha, Int. J. Quantum Chem. **75**, 889 (1999).
[18] E. G. Moroni, G. Kresse, J. Hafner, and J. Furthmüller, Phys. Rev. B **56**, 15 629 (1997).
[19] D. Porezag, M. R. Pederson, and A. Y. Liu, Phys. Rev. B **60**, 14 132 (1999).
[20] J.-H. Cho and M. Scheffler, Phys. Rev. B **53**, 10 685 (1996).
[21] S. G. Louie, S. Froyen, and M. L. Cohen, Phys. Rev. B **26**, 1738 (1982).
[22] S. C. Watson and E. A. Carter, Phys. Rev. B **58**, R13 309 (1998).
[23] O. K. Andersen, Phys. Rev. B **12**, 3060 (1975).
[24] D. Bylander and L. Kleinman, Phys. Rev. B **50**, 1363 (1994).
[25] N. A. Modine, G. Zumbach, and E. Kaxiras, Phys. Rev. B **55**, 10 289 (1997).
[26] U. V. Waghmare, H. Kim, I. J. Park, N. Modine, P. Maragakis, and E. Kaxiras, Comput. Phys. Commun. **137**, 341 (2001).
[27] O. Gunnarsson and B. I. Lundqvist, Phys. Rev. B **13**, 4274 (1976).
[28] A. Zunger, Phys. Rev. B **22**, 649 (1980).
[29] G. S. Smith, N. A. Modine, U. V. Waghmare, and E. Kaxiras, J. Comput.-Aided Mater. **5**, 61 (1998).
[30] H. Kim, U. Waghmare, and E. Kaxiras (unpublished).
[31] M. Asato, A. Settels, T. Hoshino, T. Asada, S. Blügel, R. Zeller, and P. H. Dederichs, Phys. Rev. B **60**, 5202 (1999).
[32] J.-H. Cho and M.-H. Kang, Phys. Rev. B **52**, 9159 (1995).
[33] V. Cocula and E. A. Carter (unpublished).

[34] *Landolt-Börnstein: Numerical Data and Functional Relationships in Science and Technology, New Series - Vol. III/6 Structure Data of Elements and Intermetallic Phases*, edited by P. Eckerlin, H. Kandler, and A. Stegherr (Springer-Verlag, Berlin, 1971).

[35] R. F. S. Harmon, in *Landolt-Börnstein: Numerical Data and Functional Relationships in Science and Technology, New Series - Vol. III/11 Elastic, Piezoelectric, Piezooptic, Electrooptic Constants, and Nonlinear Dielectric Susceptibilities of Crystals*, edited by K.-H. Hellwege and O. Madelung (Springer-Verlag, Berlin, 1979), p. 1.

[36] M. B. Stearns, in *Landolt-Börnstein: Numerical Data and Functional Relationships in Science and Technology - Vol. 19 Magnetic Properties of Metals - Subvolume a 3d, 4d and 5d Elements, Alloys and Compounds*, edited by H. P. J. Wijn (Springer-Verlag, Berlin, 1986), p. 24.

[37] R. F. S. Harmon, in *Landolt-Börnstein: Numerical Data and Functional Relationships in Science and Technology, New Series - Vol. III/18 Elastic, Piezoelectric, Piezooptic, Electrooptic Constants, and Nonlinear Dielectric Susceptibilities of Crystals*, edited by K.-H. Hellwege and O. Madelung (Springer-Verlag, Berlin, 1984), p. 1.

[38] M. Körling and J. Häglund, Phys. Rev. B **45**, 13 293 (1992).